Micro-patterned anti-icing coatings with dual hydrophobic/hydrophilic properties

Sarra Gam-Derouich, Jean Pinson, Aazdine Lamouri, Philippe Decorse, Sébastien Bellynck, Remy Herbaut, Laurent Royon, Claire Mangeney

Journal Name

COMMUNICATION

Micro-patterned anti-icing coatings with dual hydrophobic/hydrophilic properties

Received 00th January 20xx,
Accepted 00th January 20xx

DOI: 10.1039/x0xx00000x

www.rsc.org/

Sarra Gam-Derouich,*[§] [†]Jean Pinson[†], Aazdine Lamouri,[†] Philippe Decorse,[†] Sébastien Bellynck[†], Remy Herbaut,[‡] Laurent Royon*[⊥] and Claire Mangeney *[§]

While anti-icing research has been the focus of large interest, the approaches developed so far suffer from inherent limitations, which restrict their application. Herein, we develop a new generation of coatings coupling hierarchical nano/microstructures and dual hydrophobic/hydrophilic features, leading to efficient anti-icing properties.

Ice formation and accretion on surfaces is a major concern[1] in transports (aircrafts, cars) and energy supply (wind turbines, power lines and air conditioning). Conventional solutions to prevent ice accumulation rely on chemical methods (use of deicing fluids), thermal treatments or mechanical scraping. However, these methods are usually inefficient, costly and environmentally harmful. To overcome these limitations, surface engineering using bio-inspired anti-icing strategies have been considered[2,3,4]. A common strategy consists to trap air in surface textures to yield superhydrophobic surfaces[5,6] inspired by lotus leaves, able to promote timely removal of incoming water before freezing occurs. However, recent works have shown that frost can build up within the micro/nanostructured features of superhydrophobic surfaces under subzero conditions, leading to the anchoring of ice, which in turn results in the increase of ice adhesion during icing/deicing cycles[7,8]. An alternative strategy relies on the preparation of slippery liquid-infused porous surface (SLIPS), inspired by the slippery peristome surface of Nepenthes pitcher plants, trapping liquid as a lubricating layer between solid surfaces and accreted ice to reduce their interaction[9,10]. Self-sustainable lubricating layers based on hygroscopic polymers generating aqueous lubricating water were shown to be of particular interest[11]. Moreover, the introduction of heat mediators based on magnetic nanoparticles in SLIPS was shown to impart new active thermal deicing properties to the coatings, in addition to their passive anti-icing capacity[12]. However, few works have focused on anti-icing coatings combining hydrophilic and hydrophobic components. Although this strategy has proven to be efficient[13], the elaboration of robust binary coatings offering a spatial control of the segregation between the hydrophilic and hydrophobic components at the microscale remains challenging. We fill this gap in the present paper by designing a new generation of chemically-patterned binary coating, combining hydrophobic and hydrophilic features. The binary coatings, with micro and nanoscale features, were elaborated using a threefold strategy, combining (i) chemical nanostructuration, to achieve large scale hierarchical nanostructures on metallic surfaces, (ii) diazonium salt chemistry[14] to promote stable interfacial links between the coating and the surface and (iii) controlled/living radical iniferter photopolymerization[15], enabling the preparation of block copolymers by sequential monomer addition and the generation of controlled high-resolution patterns using a photomask. As a proof of concept, the anti-icing coatings were grafted on the surface of nano-textured copper disks. A bifunctional linker molecule was chosen, bearing aryl diazonium coupling agents for anchoring on the copper surface and iniferter terminated groups, for initiating the growth of polymer chains (see Figure 1). Highly hydrophilic polymer brushes of acrylic acid (AA) were first grown from the copper surface under UV light. The diethyldithiocarbamil groups remaining at the ends of the growing tethered chains could then be exploited to reinitiate the photopolymerization of perfluoroalkylmethacrylate (PF) from the surface, under a photomask, yielding spatially controlled hydrophobic brush patterns. The modified surfaces were characterized by scanning electron microscopy (SEM), atomic force microscopy (AFM) and X-ray photoelectron spectroscopy (XPS). Although the elaboration of the binary coating required a multi-step procedure, the grafting reactions were performed at room temperature, without any energy input, providing a simple and readily scalable method to create patterned binary coatings.

[a,§] *Lab Chim & Biochim Pharmacolog & Toxicol, University Paris Descartes, F-75006 Paris, (France). E-mail : claire.mangeney@parisdescartes.fr*
[b,†] *ITODYS, UMR 8601, University Paris Diderot, 75013 Paris (France).*
[c,‡] *MSC, University Paris Diderot, 75013 Paris (France)*
[d,⊥] *LIED, UMR 8236, University Paris Diderot, 75013 Paris (France). E-mail: Laurent.royon@univ-paris-diderot.fr*
[e,†] *† Footnotes relating to the title and/or authors should appear here.*
[f] *Electronic Supplementary Information (ESI) available. See DOI: 10.1039/x0xx00000x*

Moreover, since aryl diazonium salts provide covalent bonds between the grafted aryl layers and copper substrates, as demonstrated previously[16], the functional coatings should be mechanically robust and durable. Their anti-icing properties were then evaluated in a specifically designed chamber with controlled temperature and humidity to determine freezing delay times and supercooling temperature. The results obtained in the present work highlight the efficiency of the diazonium salt chemistry coupled to the photo-iniferter polymerization method to design stable and strongly attached, patterned binary coatings combining hydrophobic and hydrophilic properties. This strategy opens up new opportunities for the preparation of anti-icing coatings coupling dual surface properties.

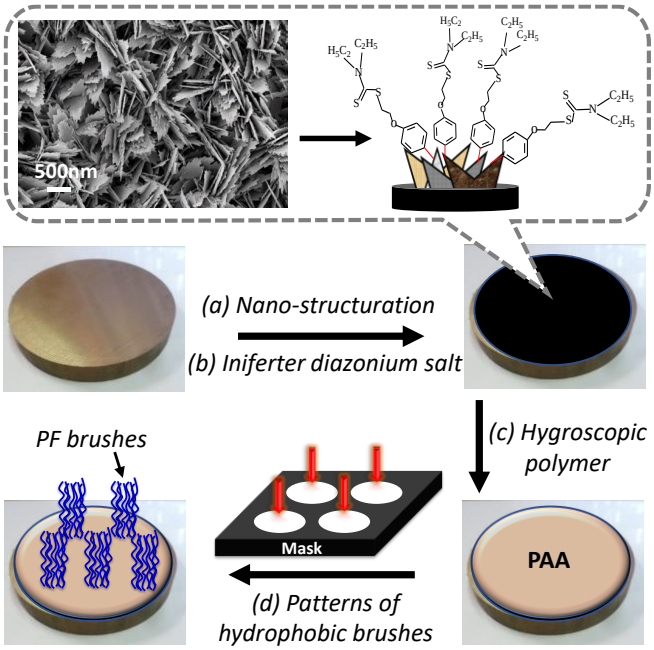

Figure 1. Schematic representation of the multi-step procedure for (a) the preparation of nano-textured Cu disks, (b) their functionalization by iniferter-based diazonium salts, (c) the grafting of hygroscopic PAA layers and (d) the photodeposition of hydrophobic (PF) polymer brush patterns.

The nanostructuration of the copper disks was performed via a simple chemical oxidation process consisting in immersing them into a hot alkaline solution (see details of the experiments in SI). As described previously[17], this procedure leads to the formation of surface nanostructures of $CuO/Cu(OH)_2$, with typical heights of h ≈ 500 nm (Fig. 2a). The spontaneous grafting of the iniferter layer derived from the diazonium salt at the surface of nanostructured copper disks was performed by simply incubating the substrates with the corresponding diazonium salt in water at room temperature during 5 h. Figure 2b shows that this functionalization treatment with the diazonium salt does not alter the initial sharp CuO structures. Interestingly, the polymerization steps preserve the nanostructure features but introduce a supplementary nanoscale roughness with polymer nodules covering entirely the knife-like CuO structures (see Figure 2c). The living character of the iniferter method was exploited to generate controlled patterns of PF blocks from the grafted PAA layer, using a photomask. To reveal the hierarchical structuration of the surface, microscopy images were recorded using optical microscopy, SEM and AFM (see Fig. 2d and Fig. S2). They clearly reveal circular micropatterns regularly arranged on top of the nanostructured copper surface. These features represent the negative image of the photomask reproduced on the substrate. The diameter of the micropatterns are of *ca.* 800 µm, which fits precisely to the hole diameter of the photomask. This confirms the presence of micropatterns of PF hydrophobic blocks on top of the PAA hydrophilic layer. It is noteworthy that the size and shape of the patterns should be easily tailored by simply changing the characteristic structures of the photomask.

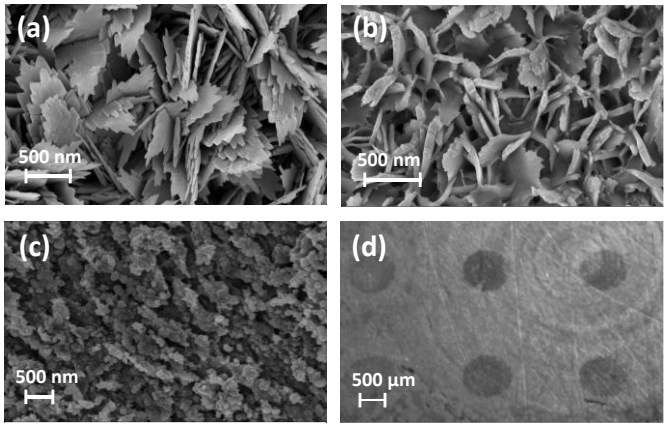

Figure 2. SEM characterization of the copper disks (a) after nanostructuration, showing the blade structure of the oxide. The sharp, knife-like CuO structures display characteristic heights, h ≈ 500 nm. (b) After grafting of the iniferter layer derived from diazonium salt. (c) After the two-step grafting of PAA and PF. (d) Optical image of the binary coating with hydrophobic PF circular micropatterns regularly arranged on top of the hydrophilic PAA layer. The diameter of the micropatterns are of *ca.* 800 µm, which fits precisely to the hole diameter in the photomask.

The various structuration and grafting steps were also investigated using XPS. The Cu2p high resolution spectra (Figure S3) confirm the oxidation of the surface during the chemical process of nanostructuration, with a shift of ~ 2.5 eV of the $Cu2p_{3/2}$ and $Cu2p_{1/2}$ peaks towards the high binding energies and the appearance of two characteristic shake-up satellite peaks. This observation is in line with previous results reporting the formation of CuO and/or $Cu(OH)_2$ nanostructures during the chemical oxidation process[18]. The grafting of the iniferter-derived diazonium salt layer was evidenced by the appearance of new peaks associated to N (N1s at *ca.* 400 eV) and S (S2p at *ca.* 164 eV, shown in Fig. 3a). The XPS analysis of the binary coating reveals the appearance of a high intensity fluorine signal related to the perfluoroalkyl polymer overlayer (see Fig. 3b). Interestingly, the C1s spectra (see Figure 3c-f) are strongly modified after functionalization. In all spectra, a main component is observed at 285 eV, related to C-C and C-H carbons. For the unfunctionalized Cu surface, the presence of

this component is probably due to adventitious contamination. After iniferter grafting, two new components at 286.4 and 288.2 eV appear, related to C-S/C-N and S-C=S, respectively. A shake-up satellite peak (π-π* transition) is also detected at *ca.* 291 eV, characteristic of the grafting of aryl layers derived from diazonium salts. The first polymerization step leads to a new peak at 289 eV related to the PAA layer while the second polymerization step generates a high-energy peak centered at 291.5 eV due to the CF_2 groups from the PF overlayer.

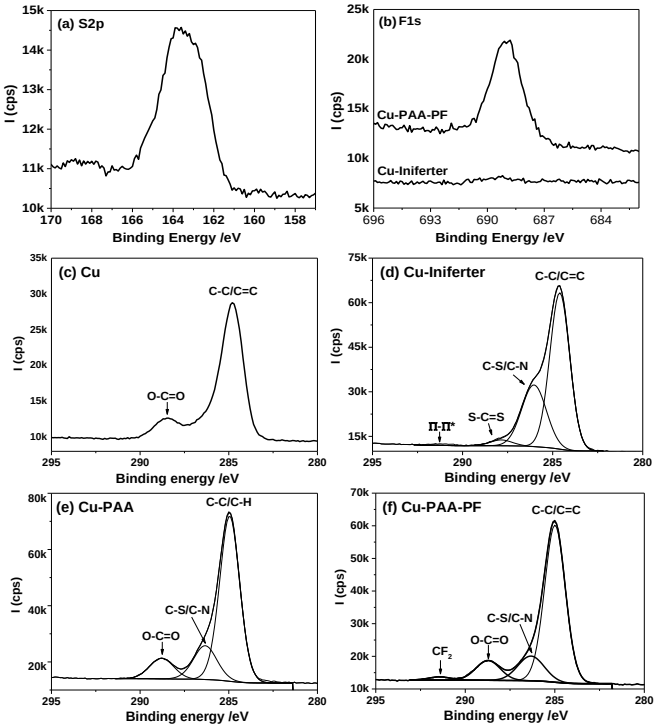

Figure 3. XPS spectra of the nanostructured copper surfaces. (a) High resolution S2p spectrum of Cu-Iniferter; (b) High resolution F1s spectra of Cu-Iniferter and Cu-PAA-PF. High resolution C1s spectra of (c) unfunctionalized Cu (d) after grafting of the iniferter; (e) after the first polymerization step leading to the grafting of PAA and (f) after the second polymerization step leading to a block copolymer of PAA-PF, with PF on the top.

The wettability properties of the Cu surfaces after nanostructuration and polymer grafting were investigated by measuring the static water contact angles (WCA) (see Fig. 4). The nanostructuration process makes the surface superhydrophilic with a WCA < 10° while the grafting of PAA increases it to 40°. After the second step of polymerization, the presence of the PF overlayer induces a further increase of the WCA to 110°, in agreement with the hydrophobic character of the grafted layers. The anti-icing properties of the nanostructured Cu-PAA-PF surfaces were investigated in an experimental chamber maintained at controlled humidity (H=30%) and temperature (see Exp. Section). Several parameters were studied including the freezing temperature of water droplets, the delay before freezing and the effect of multiple thermal icing/deicing cycles.

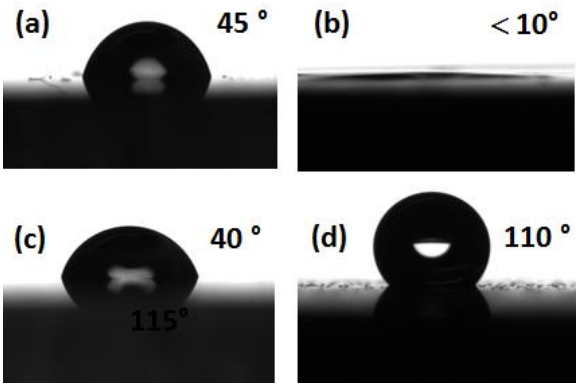

Figure 4. Goniometer contact angle measurement images and the corresponding water contact angle (WCA) on (a) smooth unmodified Cu; (b) Nanostructured Cu; (c) Nanostructured Cu-PAA and (d) Nanostructured Cu-PAA-PF. The images represent the advancing contact angles for each case.

The freezing process was recorded by an infrared camera, placed on the top and a CCD, placed on the side. All samples were simultaneously cooled down to -20°C, at a constant cooling rate of 1,2°C/min, starting from an ambient temperature of 18°C. The aim is to observe the trends induced by the chemistry and morphological surface modification on the delay time. Figure 5 compares the temperature decrease *vs* time of the droplets (100 µL) deposited on the reference unmodified copper surface and on Cu-PAA-PF. The cooling curves have a similar shape for all surfaces: (i) before the freezing occurs, the temperature decreases linearly with time; (ii) then, a fast increase of the temperature to 0°C is observed, which can be associated to the phenomena of recalescence[19].

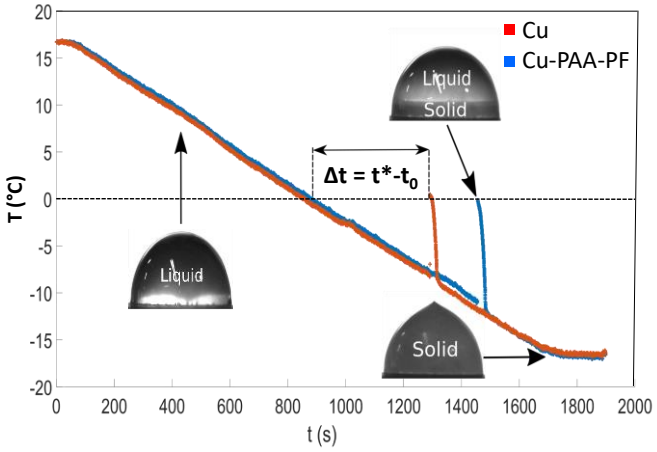

Figure 5. Temperature of sessile droplets (100 µL) monitored by IR camera as function of time (after 10 cycles). The drop profiles, recorded by the CCD camera, are added as a guide.

This jump of the temperature of water measured by the IR camera coincides with a change in the optical appearance of the droplet observed in the CCD frames. This corresponds to the freezing onset, which occurs at a time noted t*, where a crystal nucleus is born and leads to the beginning of the

freezing process. The latent heat of solidification is then released until the droplet becomes completely frozen. The supercooling temperatures defined as $\Delta T = T_{crystallisation} - T_{melting}$, were reached in the range of - 5°C to -11°C. The supercooling delay time was defined as $\Delta t = t^* - t_0$, where t_0 is the time when the droplet reaches the melting point 0°C. Figure 6 shows the mean delay times Δt, obtained from twenty measurements on bare and Cu-PAA-PF surfaces, as a function of the number of thermal cycles. The freezing delays of water droplets recorded on Cu-PAA-PF were found to be superior to the values recorded on bare Cu, for all cycles. It remained stable over 8 min, even after 20 thermal cycles, confirming the stability of the grafted binary coating. Regarding the supercooling temperature, displayed as a function of the number of cycles in Figure S5, it appeared to be significantly lower for Cu-PAA-PF compared to the reference Cu surface. It remained at around -10°C even after 20 cycles, preventing ice formation above this temperature. Generally, the comparison of Cu-PAA-PF with more conventional surfaces, such as bare Cu, planar Cu-PF, nanostructured Cu-PF and nanostructured Cu-PAA (see Fig. S6) indicated that the micro/nano-structuration of Cu and its functionalization by patterned binary PAA-PF coatings improved sustainably the freezing delay times, over multiple freezing/defreezing cycles. The combination of micro/nano-structuration and dual hydrophobic/hydrophilic features are thus key elements to improve the anti-icing properties compared to untreated Cu, with increased freezing delays, lower supercooling temperature and high stability with time.

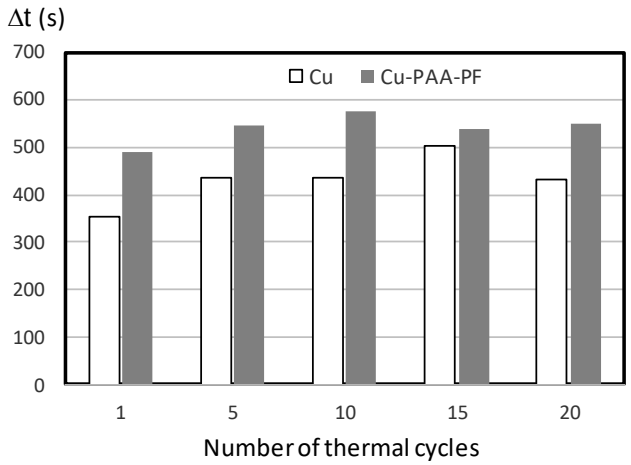

Figure 6. Delay times of freezing (Δt) as a function of the number of cycles. The white columns report the values obtained for the reference bare Cu and the grey columns report the values recorded on Cu-PAA-PF surfaces.

Conclusions

In summary, we have developed a new generation of anti-icing coatings, based on hydrophobic polymer brush patterns grafted on top of hydrophilic layers. The binary coatings were grafted on the surface of nano-textured copper disks and patterned at the microscale using controlled living radical photopolymerization from iniferter layers derived from diazonium salts. The advantages of this strategy include the formation of stable interfacial links between the coating and the surface and the possibility to prepare high-resolution patterns of block copolymers using a photomask. Moreover, it can be applied to a wide range of materials and it is scalable to the functionalization of large area. The potentialities of this strategy to impart anti-icing properties were evaluated in a specifically designed chamber with controlled temperature and humidity. The binary coatings were shown to enhance the freezing delays and decrease the supercooling temperature of the nanostructured copper surface, over extended periods of time and several cycles of frosting/defrosting. This strategy thus offers promising prospects for the functionalization of surfaces and provides a new way to attach anti-icing coatings coupling hierarchical nano/microstructures and dual surface properties on various kinds of surfaces.

Conflicts of interest

There are no conflicts to declare.

Aknowledgements

This work was supported by French state funds managed by the ANR within the Investissements d'Avenir programme under reference ANR-15-CE08-0031. Authors acknowledge Dr. Jérôme Médard for the AFM images.

References

1 T. Bartels-Rausch, *Nature*, 2013, **494**, 27–29.
2 M. J. Kreder, J. Alvarenga, P. Kim and J. Aizenberg, *Nat. Rev. Mater*., 2016, **1**, 15003.
3 J. Lv, Y. Song, L. Jiang and J. Wang, *ACS Nano*, 2014, **8**, 3152–3169.
4 S. Zhang, J. Huang, Y. Cheng, H. Yang, Z. Chen and Y. Lai, *Small*, 2017, **13**, 1701867.
5 H.X. Wang, Y.H. Xue, J. Ding, L.F. Feng, X.G. Wang and T. Lin, *Angew. Chem. Int. Ed.*, 2011, **50**, 11433–11436.
6 (a) A. Checco, A. Rahman and C.T. Black, *Adv. Mater*., 2014, **26**, 886–891; (b) Y. Tang, Q. Zhang, X. Zhan and F. Chen, *Soft Matter,* 2015, **11**, 4540-4550 ; (c) T. Cheng, R. He, Q. Zhang, X. Zhan and F. Chen, *J. Mater. Chem. A*, 2015, **3**, 21637–21646.
7 J. Chen, J. Liu, M. He, K. Li, D. Cui, Q. Zhang, X. Zeng, Y. Zhang, J. Wang and Y. Song, *Appl. Phys. Lett*., 2012, **101**, No. 111603.
8 T. Maitra, S. Jung, M.E. Giger, V. Kandrical, T. Ruesch and D. Poulikakos, *Adv. Mater. Interf.*, 2015, **2**, No. 1500330.
9 (a) T. S. Wong, S. H. Kang, S. K. Y. Tang, E. J. Smythe, B. D. Hatton, A. Grinthal and J. Aizenberg, *Nature,* 2011, **477**, 443-447; (b) C. Wei, B. Jin, Q. Zhang, X. Zhan and F. Chen, *J. Alloys Compd*., 2018, **765**, 721e730.
10 P. Kim, T. S. Wong, J. Alvarenga, M. J. Kreder, W. E. Adorno-Martinez and J. Aizenberg, *ACS Nano*, 2012, **6**, 6569–6577.
11 (a) J. Chen, R. Dou, D. Cui, Q. Zhang, Y. Zhang, F. Xu, X. Zhou, J. Wang, Y. Song and L. Jiang, *ACS Appl. Mater.*

Interfaces, 2013, **5**, 4026–4030; (b) J. Chen, K. Li, S. Wu, J. Liu, K. Liu and Q. Fan, *ACS Omega*, 2017, **2**, 2047-2054.
12 G. Zhang, Q. Zhang, T. Cheng, X. Zhan and F. Chen, *Langmuir*, 2018, **34**, 4052−4058.
13 C. Li, X. Li, C. Tao, L. Ren, Y. Zhao, S. Bai and X. Yuan, *ACS Appl. Mater. Interfaces*, 2017, **9**, 22959−22969.
14 (a) J. Pinson and F. Podvorica, *Chem. Soc. Rev*., 2005, **34**, 429-439; (b) M. M. Chehimi, J. Pinson and F. Podvorica, In Electroanalytical Chemistry (Eds.: A.J. Bard, C.G. Gzoski), CRC Press: Boca Raton, FL, 2016, pp. 115−224; (c) R. Ahmad, L. Boubekeur-Lecaque, M. Nguyen, S. Lau-Truong, A. Lamouri, P. Decorse, A. Galtayries, J. Pinson, N. Felidj and C. Mangeney, *J. Phys. Chem. C*, 2014, **118**, 19098-19105 ; (d) J. J. Gooding, F. Mearns, W. R. Yang and J. Q. Liu, *Electroanalysis*, 2003, **15**, 81-96; (e) A. Laforgue, T. Addou and D. Belanger, *Langmuir*, 2005, **21**, 6855-6865; (f) F. Zen, M. D. Angione, J. A. Behan, R. J. Cullen, T. Duff, J. M. Vasconcelos, E. M.; Scanlan and P. E. Colavita, *Sci. Rep*., 2016, **6**, 24840 ; (g) C. Jiang, M. Tanzirul Alam, S. M. Silva, S. Taufik, S. Fan and J. J. Gooding, *ACS Sens*, 2016, **1**, 1432–1438.
15 (a) T. Otsu, *J Polym Sci Part A Polym Chem,* 2000, **38**, 2121e36; (b) E. M. Benetti, S. Zapotoczny and G.J. Vancso, *Adv. Mater*., 2007, **19**, 268e71. (c) R. Ahmad, N. Félidj, L. Boubekeur-Lecaque, S. Lau-Truong, S. Gam-Derouich, P. Decorse, A. Lamouri and C. Mangeney, *Chem. Comm*., 2015, **51**, 9678-9681; (d) R. Ahmad, A. Mocaer, S. Gam-Derouich, A. Lamouri, H. Lecoq, P. Decorse, P. Brunet and C. Mangeney, *Polymer*, 2015, **57**, 12-20.
16 (a) B.L. Hurley and R.L. McCreery, *J. Electrochem Soc*., 2004, **151**, B252-B259; (b) M.-C. Bernard, A. Chaussé, E. Cabet-Deliry, M. M. Chehimi, J. Pinson, F. Podvorica and C. Vautrin-Ul, *Chem. Mater.,* 2003, **15***,* 3450-3462; (c) P. Doppelt, G. Hallais, J. Pinson, F. Podvorica and S. Verneyre, *Chem. Mater.,* 2007, **19***,* 4570-4575.
17 N. Miljkovic, R. Enright, Y. Nam, K. Lopez, N. Dou, J. Sack and E. N. Wang, *Nano. Lett*., 2013, **13**, 179−187.
18 O. Akhavan, R. Azimirad, S. Safad and E. Hasanie, *J. Mater. Chem.*, 2011, **21**, 9634-9640.
19 G. Chaudhary and R. Li, *Exp. Therm. Fluid Sci*., 2014, **57**, 86-93.